J Appl Electrochem (2009) 39:191–196
DOI 10.1007/s10800-008-9651-y

ORIGINAL PAPER

Preparation and evaluation of RuO_2–IrO_2, IrO_2–Pt and IrO_2–Ta_2O_5 catalysts for the oxygen evolution reaction in an SPE electrolyzer

A. Di Blasi · C. D'Urso · V. Baglio · V. Antonucci · A. S. Arico' · R. Ornelas · F. Matteucci · G. Orozco · D. Beltran · Y. Meas · L. G. Arriaga

Received: 14 November 2007 / Accepted: 15 August 2008 / Published online: 6 September 2008

Abstract IrO_2–RuO_2, IrO_2–Pt and IrO_2–Ta_2O_5 electrocatalysts were synthesized and characterized for the oxygen evolution in a Solid Polymer Electrolyte (SPE) electrolyzer. These mixtures were characterized by XRD and SEM. The anode catalyst powders were sprayed onto Nafion 117 membrane (catalyst coated membrane, CCM), using Pt catalyst at the cathode. The CCM procedure was extended to different in-house prepared catalyst formulations to evaluate if such a method could be applied to electrolyzers containing durable titanium backings. The catalyst loading at the anode was about 6 mg cm^{-2}, whereas 1 mg cm^{-2} Pt was used at the cathode. The electrochemical activity for water electrolysis was investigated in a single cell SPE electrolyzer at 80 °C. It was found that the terminal voltage obtained with Ir–Ta oxide was slightly lower than that obtained with IrO_2–Pt and IrO_2–RuO_2 at low current density (lower than 0.15 A cm^{-2}). At higher current density, the IrO_2–Pt and IrO_2–RuO_2 catalysts performed better than Ir–Ta oxide.

Keywords Oxygen evolution · Water electrolysis · Solid polymer electrolyte · Oxides

A. Di Blasi · C. D'Urso · V. Baglio · V. Antonucci · A. S. Arico'
CNR-ITAE, Via Salita S. Lucia sopra Contesse, 5-98126 Messina, Italy

R. Ornelas · F. Matteucci
Tozzi Renewable Energy SpA, Via Zuccherificio, 10-48010 Mezzano (RA), Italy

G. Orozco · D. Beltran · Y. Meas · L. G. Arriaga (✉)
Centro de Investigación y Desarrollo Tecnológico en Electroquímica S.C., c.p.76700 Sanfandila, Querétaro, Mexico
e-mail: larriaga@cideteq.mx

1 Introduction

Presently, hydrogen production is carried out by reforming of different hydrocarbons (from methane to naphthas). Reforming reactions are highly endothermic. Therefore, it is necessary to carry out the process by combustion of gas or oil. Significant amounts of CO_2 are generated by both the combustion and the reforming processes which will markedly affect the environment when hydrogen is produced on a large scale [1–3]. The production of hydrogen using renewable resources, such as electrolysis and photoelectrolysis reduces significantly the amount of pollutants emitted since these processes are essentially characterized by zero-emissions.

Two types of hydrogen generators by electrolysis process are commercially available, i.e. alkaline electrolyzer (EA) and solid polymer electrolyte electrolyzer (SPE). Alkaline electrolyzers are more popular because the technology is well developed, and several suppliers are available (Stuart, Hydrogen Systems, Norsk Hydro Electrolyzers). The operating temperature and pressure of both types of electrolyzers are similar. However, compared with alkaline electrolyzers the SPE systems offer some advantages including higher hydrogen purity (i.e. no need for a clean-up process), no corrosive electrolyte, lower energy consumption and it is not necessary to apply a voltage to avoid corrosion when the system is not in operation. Furthermore, a SPE electrolyzer is compact and its electrolyte is chemically stable, whereas the KOH in alkaline electrolyzers is susceptible to carbonation.

Oxygen evolution occurs on noble metal catalysts (e.g., Pt, Au, Ir, Rh, Ru, Ag), but metal oxides (eg., RuO_2, IrO_2) are generally more active electrocatalysts for this reaction than the metal electrodes. Several factors influence the electrocatalytic evolution of oxygen including. the

crystal-field stabilization energy, mixed and doped oxides, dispersion, crystallinity, and crystallite size [4]. IrO_2 catalyst has been examined as an anode (oxygen evolution electrode) in SPE electrolyzers [5]. IrO_2 and RuO_2 are well established as electrocatalysts in many industrial electrochemical processes in the form of dimensionally stable anodes [2]. IrO_2 exhibits high corrosion resistant properties but slightly lower electrocatalytic activity than RuO_2 [6]. Most dimensionally stable anode electrodes are prepared by thermal decomposition of metal precursors onto titanium substrates [7]. This method is unsuitable for SPE electrolyzers due to the difficulty of obtaining good contacts between the electrocatalytic layer and the membrane. Alternatively, the anode catalyst is deposited onto the electrode backing or diffusion layer, often formed with carbonaceous materials [5, 8–11]. There are two constraints associated to this procedure. First, the carbonaceous materials are not stable during prolonged operation at elevated potentials and, second, the triple phase formation usually requires hot bonding to the membrane in a press that may cause membrane damage and degradation. To obtain a proper electrocatalytic layer on the membrane, pre-prepared powders may be applied as an ink onto the membrane [12]. The ink may contain both the catalyst and ionomer to enlarge the triple-phase boundary within the catalytic layer. This approach is presently used in polymer electrolyte fuel cells and it is called catalyst coated membrane (CCM) [13, 14]. The diffusion/backing layer is added subsequently when the membrane-electrode assembly (MEA) is installed in the cell. The CCM method was recently investigated by Zhang et al. [14] for manufacturing a membrane electrode assembly for SPE electrolyzer. The method was assessed by using just one catalyst formulation. In this work we have extended the CCM procedure to various catalytic formulations to evaluate if such a method could be applicable to electrolyzers containing durable titanium backings and how the most promising catalytic formulation behaves for oxygen evolution in a wide range of current densities.

2 Experimental

2.1 Preparation of IrO_2–RuO_2 electrocatalyst

Appropriate amounts of $(NH_4)_2IrCl_6$ (Aldrich) and $(NH_4)_2RuCl_6$ (Aldrich) were dissolved in deionised water, in order to prepare an atomic ratio Ir:Ru = 50:50. The aqueous solution was then heated (80 °C) in air and stirred for 2 h. The resulting paste was pulverized and then washed three times with deionised water, before being dried in air for 3 h at 80 °C. The dry powder was then annealed in air at 500 °C for 2 h, using a heating rate of 3 °C min^{-1}.

2.2 Preparation of IrO_2–Pt electrocatalysts

The preparation of IrO_2–Pt was carried out by incipient wetness technique which consists of the impregnation of commercial amorphous-like IrO_2 (Spectrum) onto a commercial Pt black (Johnson Matthey). The electrocatalyst was prepared at 50:50 atomic ratio of Ir:Pt.

2.3 Preparation of IrO_2–Ta_2O_5 electrocatalyst

The preparation of Ir–Ta oxide was carried out by dissolving $(NH_4)_2IrCl_6 \times H_2O$ (Strem Chemical) in HCl with an ultrasonic stirring system. This solution was mixed with tantalum (V) chloride, anhydrous (99.9% Ta) ($TaCl_5$) (Strem Chemical), in order to prepare an atomic ratio Ir:Ta = 70:30. This solution was then heated at 80 °C in air for 2 h to precipitate a powder material. The powder was annealed in air at 500 °C.

2.4 Preparation of Pt/C electrode

A commercial 30% Pt/Vulcan XC-72 (E-TEK, PEMEAS, Boston, USA) was used as the catalyst for H_2 evolution. The electrode was prepared by directly mixing in an ultrasonic bath, a suspension of Nafion ionomer in water with the catalyst powder (catalyst/dry ionomer = 2/1 wt.). The paste obtained was spread on carbon cloth backings (GDL ELAT from E-TEK).

2.5 Physico-chemical characterization

The powders were characterized by X-Ray Diffraction (XRD), X-Ray Fluorescence (XRF) and Scanning Electron Microscopy (SEM). X-ray diffraction analysis was performed on dry electrocatalytic powders using a Philips X-Pert 3710 diffractometer with Kα line of Copper (CuKα). This diffractometer operates at 40 kV and 30 mA, step time of 0.5° 2θ min^{-1}, angular resolution of 0.005° 2θ. The diffraction patterns were fitted to JCPDS (Joint Committee on Powder Diffraction Standards) and crystal size distribution was calculated using LBA (line broadening analysis).

X-ray fluorescence analysis of the catalysts was carried out by a Bruker AXS S4 Explorer spectrometer operating at 1 kW. The spectrometer was equipped with a Rh X-ray source, a LiF crystal analyzer and a 0.12° divergence collimator.

A Philips XL 30 scanning electron microscope was used for SEM-EDX analysis of the catalysts.

2.6 Preparation of membrane and electrode assembly (MEA)

The oxygen evolution catalysts were directly deposited onto one side of Nafion 117 (Du Pont) membrane by spray

technique. Inks were composed of aqueous dispersions of catalyst, deionised water, Nafion solution (5% Aldrich) and anhydrous Ethylic alcohol (Carlo Erba). The loading of anode catalyst was about 6 mg cm^{-2}, while the cathode loading was 1 mg cm^{-2} Pt using a 30% Pt/C (E-TEK) as catalyst. The ionomer (Nafion, Ion Power) content was 33% by weight in the catalyst layer after drying. A Nafion 117 (Ion Power) membrane was used as solid polymer electrolyte. Instead of carbon cloth as a backing layer, a titanium grid was used as a diffusion layer and current collector for the anode to avoid corrosion. To facilitate gas evolution, the titanium grid was immersed in a water/FEP (1:1) (Dyneon FEP 6300 RG) solution for 1 min and then it was dried in an oven. Sintering was carried out at 350 °C for 30 min. MEAs were directly prepared in the cell housing by tightening at 9 Nm using a dynamometric wrench.

2.7 Evaluation of water electrolysis performance

The SPE electrolyzer performance was evaluated at 80 °C. Heated deionised water, which was circulated by a pump at a flow rate of 2 ml min^{-1}, was supplied to both electrodes. The water temperature was maintained at 10 °C higher than the cell temperature. Cell potentials were measured as a function of current density with an Autolab PGSTAT 302 Potentiostat/Galvanostat (Metrohm).

3 Results and discussion

3.1 IrO_2–RuO_2

XRD analyses were carried out on the anode catalysts. Figure 1 shows XRD patterns of the precursor powder after calcination at 500 °C for 2 h. The XRD peaks were assigned to IrO_2 and RuO_2. No presence of Ir and Ru in a metallic form was found. The crystalline structure was assigned to tetragonal rutile. The crystallite size was estimated at around 10–12 nm based on the broadening of three principal peaks (28.1, 35.12 and 54.07°) using the Scherrer equation.

A SEM image of IrO_2–RuO_2 is shown in Fig. 2. A porous morphology was observed with two different phases, one corresponding to IrO_2 and the other typical of RuO_2. The EDX analysis allowed for the small particles of the same size to be identified by XRD to be composed of IrO_2. Agglomerates of larger sized particles appeared to be mainly composed of RuO_2.

Table 1 shows the X-ray fluorescence data for the IrO_2–RuO_2 catalyst. From this analysis, it was determined that the Ru concentration was slightly larger than Ir in the catalyst after calcination and washing, whereas their concentrations were equal in the precursor.

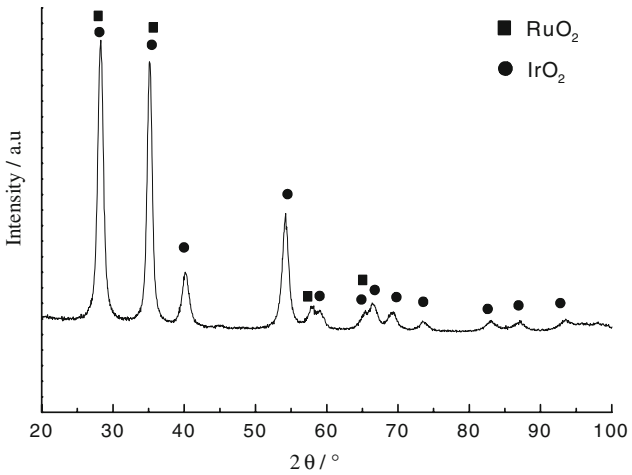

Fig. 1 X-ray diffraction patterns of IrO_2–RuO_2 powder calcined at 500 °C

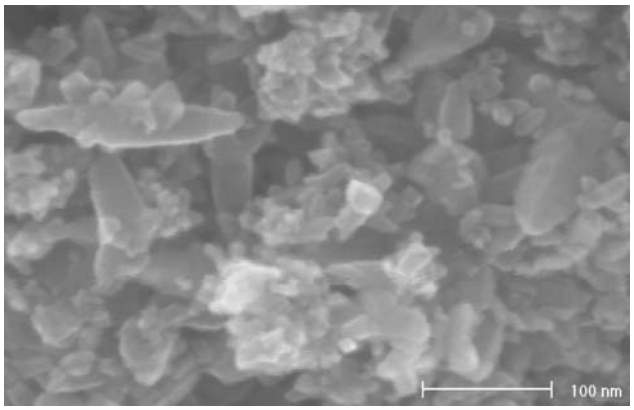

Fig. 2 SEM image of IrO_2–RuO_2 calcined at 500 °C

Table 1 Physico-chemical characteristics of IrO_2–RuO_2, IrO_2–Pt and IrO_2–Ta_2O_5 catalysts

Catalysts	Composition from XRF (wt.%)				Particle size from XRD (nm)
	Ru	Ir	Pt	Ta	
IrO_2–RuO_2	53.4	44.5	–	–	10–12
IrO_2–Pt	–	56.94	42.57	–	6 (Pt)
IrO_2–Ta_2O_5	–	73.4	–	19.3	–

3.2 IrO_2–Pt

Figure 3 shows a comparison among IrO_2, IrO_2–Pt and Pt. IrO_2–Pt shows the typical face centered cubic structure of Pt and a particle size of 6.1 nm (the same of Pt black from Johnson–Matthey). Moreover, by comparing Pt and IrO_2–Pt, the latter shows a little shoulder at about 35° 2θ due to the presence of IrO_2. At 2θ degrees higher than 40°, IrO_2–Pt shows small peaks of metallic Ir which are also present in the commercial IrO_2. An SEM image of IrO_2–Pt is

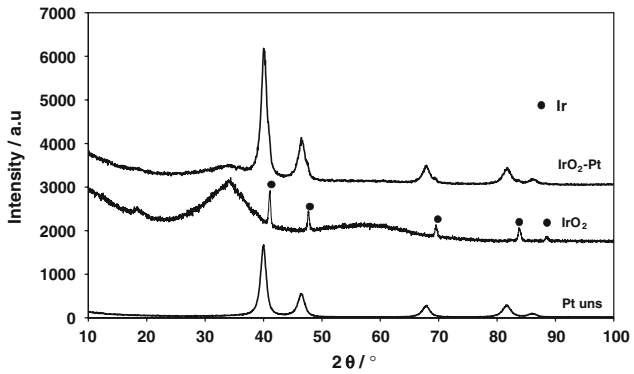

Fig. 3 X-ray diffraction patterns of IrO_2, IrO_2–Pt and Pt

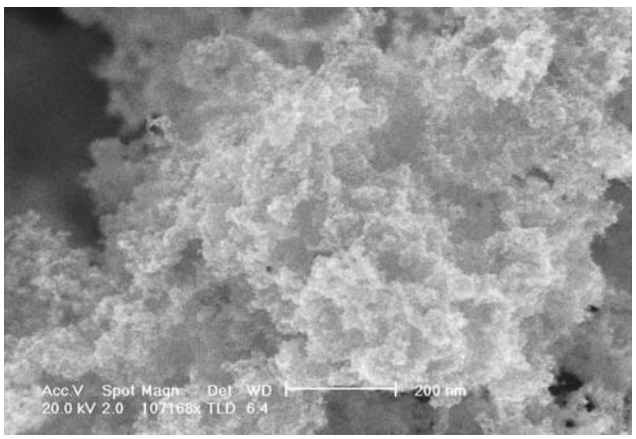

Fig. 4 SEM image of IrO_2–Pt

shown in Fig. 4. A porous morphology typical of Pt particles is evident.

3.3 IrO_2–Ta_2O_5

The X-ray diffraction pattern of Ir–Ta oxide catalyst is shown in Fig. 5, with mainly an amorphous phase, in agreement with the results of Rolewicz et al. and Murakami et al. [7, 15]. The SEM image of IrO_2–Ta_2O_5 (Fig. 6) showed mainly the presence of large agglomerates of different sizes, well bonded each other.

Table 1 shows the X-ray fluorescence results of the Ir–Ta oxide with an atomic percentage Ir/Ta = 4/1. Thus, a minimal difference with respect to the atomic ratio used in the synthesis procedure was found.

3.4 Evaluation of water electrolysis cell performance

Figure 7 shows the terminal voltage versus current density curves for electrolysis cells using IrO_2–RuO_2, Ir–Ta oxide and IrO_2–Pt as anode electrodes at 80 °C. A 30% Pt/Vulcan (E-TEK) was used as the cathode catalyst in all experiments. A Teflonized Ti grid was used as the current

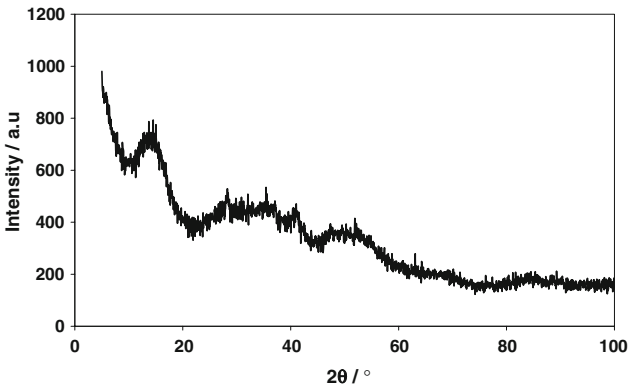

Fig. 5 X-ray diffraction patterns of IrO_2–Ta_2O_5 powder calcined at 500 °C

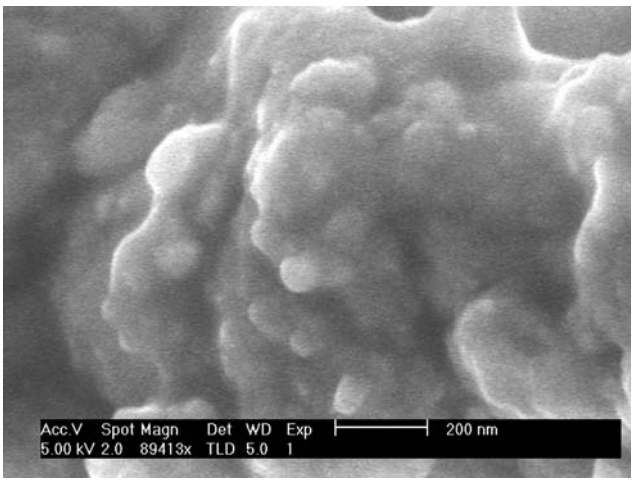

Fig. 6 SEM image of IrO_2–Ta_2O_5

collector in the anodic compartment and a carbon cloth coated with a diffusion layer (ELAT from E-TEK) was used as the cathode current collector. During the electrolysis operation, the terminal voltage of the IrTa oxide-based cell was slightly lower than that of the IrO_2–Pt and IrO_2–RuO_2 cells at current densities lower than 0.15 A cm^{-2}. In contrast, at current densities greater than 0.15 A cm^{-2} the behavior changed and the IrO_2–RuO_2 and IrO_2–Pt based cells produced more current than Ir–Ta oxide cell.

Since the results obtained for the three anodes were quite similar, the influence of sample variation was explored. In order to determine the sample variation for the three electrodes, a normal statistical distribution was carried out, using two different MEAs for each formulation and duplicate runs (two polarization curves) for each electrode (for a total of four experimental results) and a 95% of accuracy interval [17]. The standard error was calculated at around 2–3%. The error bars for each MEA are shown in Fig 7.

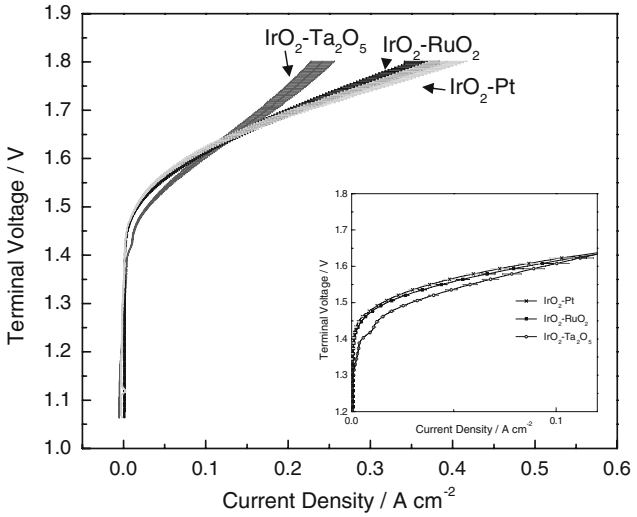

Fig. 7 Terminal voltage versus current density curves of IrO_2–RuO_2, IrO_2–Ta_2O_5 and IrO_2–Pt as anode electrodes at 80 °C. The error bars are shown for each electrode

A comparison of the electrochemical behavior in the range of polarization controlled by kinetics for the different catalysts is shown in the insert in Fig. 7. The catalyst with the best activity appears to be the Ir–Ta oxide, probably due to the higher amount of IrO_2 (70:30 atomic ratio) compared to the other catalysts (50:50 atomic ratio).

Also, the physical chemical properties resulting from the preparation procedure play an important role in determining the catalytic activity. In the present work, compared to the literature [17], a simple, fast and low cost method of preparation of an IrO_2–RuO_2 electro-catalyst was used. $IrCl_6$ and $(NH_4)_2RuCl_6$ precursors were mixed in an aqueous solution, heated to 80 °C, dried and annealed in air at 500 °C. This procedure yielded a large amount of catalytic powder per batch and, moreover, no toxic gas evolution occurred during the preparation. Unfortunately, as observed in the SEM image, RuO_2 particles appear to be very large with a consequent low surface area. This characteristic should affect the catalytic behavior. For the IrO_2–Pt catalyst, an impregnation procedure was utilized employing commercial catalysts. Thus, the surface properties could be affected by this preparation technique.

The differences in the high current region could be attributed to the presence of Ta_2O_5 that is known to be more resistive (in terms of electronic conductivity) than the other oxides used in the present study. In fact, from the slope of the I–V curve for the Ir–Ta oxide-based cell, a higher cell resistance was measured. From the observation of the SEM image of the Ir–Ta oxide, a large agglomeration was observed with a lower porosity compared to the other oxides. This could be responsible of the diffusion constraints observed for the Ir–Ta oxide cell.

The energy efficiency of the water electrolysis was evaluated at low current densities (0.01–0.2 A cm^{-2}) in order to analyze the performance of the anode catalyst without the influence of ohmic resistivity and high bubble formation. Based on terminal voltage versus current density characteristics, the efficiency of the water electrolysis can be calculated. The efficiency of water electrolysis (η_{we}) is given by the following equation:

$$\eta_{we} = \Delta H / nFE_{we} \quad (1)$$

where n is number of moles of electrons involved in the reaction, F is the faraday constant, ΔH is the enthalpy change of the reaction, E_{we} is the terminal voltage for the water electrolysis at a given current density (the higher heating value of ΔH was used). The efficiency η_{we} was calculated according to Eq. 1 at current density of 0.01 A cm^{-2} (mainly characterized by activation losses) and intermediate current densities 0.1 and 0.25 A cm^{-2} (characterized by initial ohmic losses). Table 2 shows the results for IrO_2–Pt, IrO_2–RuO_2 and IrO_2–Ta_2O_5 cells. As expected from the voltage versus current characteristics, the Ir–Ta oxide cell showed the highest efficiency (68.6%) for water electrolysis at current densities of 0.01 A cm^{-2}, whereas the IrO_2–Pt, IrO_2–RuO_2 cells showed almost the same efficiency. This may be attributed to a higher electrocatalytic response of IrTa oxide than for the other two anode electrodes. The efficiency for the three cells at 0.1 A cm^{-2} was around 60%, while for a current density of 0.25 A cm^{-2}, the Ir–Ta oxide cell showed the lowest efficiency and the IrO_2–Pt, IrO_2–RuO_2 cells showed an efficiency of about 56%. The lower performance of IrO_2–RuO_2 catalyst compared to the results reported in the literature could be due to the large particle size of RuO_2. IrO_2–Pt, which has been developed mainly for Unitized Regenerative Fuel Cells (URFCs), showed promising activity for electrolyzers, probably due to its composition with a suitable particle size (6 nm for Pt particles). The efficiency could be improved by optimizating the catalyst's

Table 2 Energy efficiency of water electrolysis at 0.01, 0.1 and 0.25 A cm^{-2} for different materials

Current density (A cm^{-2})	Anode electrode	η_{we}
0.01	IrO_2–RuO_2	66.1
	IrO_2–Ta_2O_5	**68.6**
	IrO_2–Pt	65.8
0.1	IrO_2–RuO_2	60.4
	IrO_2–Ta_2O_5	**60.7**
	IrO_2–Pt	60.2
0.25	IrO_2–RuO_2	56.7
	IrO_2–Ta_2O_5	54.2
	IrO_2–Pt	**56.9**

Bold denotes maximum value obtained

properties in terms of morphology and electronic characteristics. High cell efficiency is reported in the literature approaching 90% with optimized catalysts and with a catalyst loading around 8–10 mg cm^{-2} [8, 9, 13]. Yet, in most of these reports expensive catalyst preparation procedures were employed [17] and mainly carbonaceous materials were used as electrode backings which are neither practical nor stable. These backings are advantageous in terms of reduced ohmic drop but such carbonaceous compounds, e.g. carbon cloth, carbon paper, carbon fibers, give rise to degradation during prolonged operation. The electrochemical data in this work were obtained with durable Ti backings in order to make comparison under conditions that are similar to the industrial applications.

4 Conclusions

The energy efficiency was evaluated for the three anode electrodes (IrO_2–Ta_2O_5, IrO_2–Pt and IrO_2–RuO_2) at low current densities to compare the catalytic activity without interference from ohmic and mass transport losses. Durable Ti electrode backings were used at the anode and a CCM procedure was employed for MEA preparation. The highest efficiency at a current density of 0.01 A cm^{-2} for the different electrolysis cells was achieved for Ir–Ta oxide at 68.6%. At larger current densities IrO_2–Pt and IrO_2–RuO_2 showed better catalytic activities than Ir–Ta oxide. The ohmic drop was larger for the Ir–Ta oxide which significantly influences the behaviour of this catalyst. The poorer performance for IrO_2–RuO_2 compared to the literature is probably due to the large RuO_2 particle size. In order to evaluate these anode electrodes at higher current densities of up to 0.3 A cm^{-2}, a good electrolyzer design with low ohmic losses will be important and an appropriate diffusion backing layer will be essential.

Acknowledgements CNR-ITAE authors acknowledge Tozzi S.p.A. for financial support. L.G. Arriaga thanks CNR-ITAE and Conacyt-QROO-2005-C01-18975 for economic support.

References

1. Arriaga LG, Martínez WM, Cano U, Blud H (2007) Int J Hydrogen Energy 32:2247
2. Marshall A, Borrasen B, Hagen G, Tsypkin M, Tunold R (2005) Mater Chem Phys 94:226
3. Oberlin R, Fischer M (1986) In: Proceedings of the sixth world hydrogen energy conference on hydrogen energy progress VI. Pergamon Press, NY, USA, p 333
4. Morales SL, Arriaga LG, Cano U, Acosta R (2006) In: ECS Transactions, vol 3. Proton exchange membrane fuel cells 6. The Electrochemical Society, NJ, USA, p 115
5. Zhang Y, Wang C, Wan N, Mao Z (2007) Int J Hydrogen Energy 32:400
6. Hu J-M, Zhang J-Q, Cao CN (2004) Int J Hydrogen Energy 29:791
7. Murakami Y, Tsuchiya S, Yahikozawa K, Takasu Y (1994) Electrochim Acta 39:651
8. Ioroi T, Kitazawa N, Yasuda K, Yamamoto Y, Takenaka H (2000) J Electrochem Soc 147:2018
9. Ioroi T, Yasuda K, Siroma Z, Fujiwara N, Miyazaki Y (2002) J Power Sources 112:583
10. Yim S, Lee W, Yoon Y, Sohn Y, Park G, Yang T, Kim C (2004) Electrochim Acta 50:713
11. Yao W, Yang J, Wang J, Nuli Y (2007) Electrochem Commun 9:1029
12. Rasten E, Hagen G, Tunold R (2003) Electrochim Acta 48:3945
13. Marshall A, Borresen B, Hagen G, Tsypkin M, Tunold R (2007) Energy 32:431
14. Zhang Y, Wang C, Wan N, Liu Z, Mao Z (2007) Electrochem Commun 9:667
15. Rolewicz J, Comninellis Ch, Plattner E, Hinden J (1988) Chimia 42:75
16. Montgomery Douglas C (2002) Probabilidad y Estadistica aplicadas a la Ingenieria, 2nd edn. Limusa Wiley, Madrid, España
17. Lopez M, Schleunung A, Biberbach P (2002) Patent no. WO2005049199